| Title | Thermally-controlled spherical peptide gel architectures prepared using the pH switch method |
|---|---|
| Authors(s) | Almohammed, Sawsan, Kanoun, Mohammed Benali, Goumri-Said, Souraya, Alam, Mir Waqas, Fularz, Agata, Alnaim, Abdullah, Rice, James H., Rodriguez, Brian J. |
| Publication date | 2022-03-23 |
| Publication information | Almohammed, Sawsan, Mohammed Benali Kanoun, Souraya Goumri-Said, Mir Waqas Alam, Agata Fularz, Abdullah Alnaim, James H. Rice, and Brian J. Rodriguez. "Thermally-Controlled Spherical Peptide Gel Architectures Prepared Using the pH Switch Method" 115, no. 3 (March 23, 2022). |
| Publisher | Wiley |
| Item record/more information | http://hdl.handle.net/10197/25219 |
| Publisher's version (DOI) | 10.1002/pep2.24304 |

**ARTICLE**

# Thermally-controlled spherical peptide gel architectures prepared using the pH switch method

Sawsan Almohammed[1,2] | Mohammed Benali Kanoun[3] | Souraya Goumri-Said[4] | Mir Waqas Alam[3] | Agata Fularz[1] | Abdullah Alnaim[3] | James H. Rice[1] | Brian J. Rodriguez[1,2]

[1]School of Physics, University College Dublin, Dublin, Ireland

[2]Conway Institute of Biomolecular and Biomedical Research, University College Dublin, Dublin, Ireland

[3]Department of Physics, College of Science, King Faisal University, Al-Ahsa, Saudi Arabia

[4]Physics Department, College of Science and General Studies, Alfaisal University, Riyadh, Saudi Arabia

**Correspondence**

James H. Rice, Brian J. Rodriguez and Sawsan Almohammed, School of Physics, University College Dublin, Belfield, Dublin D04 V1W8, Ireland.
Email: james.rice@ucd.ie; brian.rodriguez@ucd.ie and sawsan.f.almohammed@gmail.com

**Abstract**

Self-assembling nanostructured peptide gels are promising materials for sensing, drug delivery, and energy harvesting. Of particular interest are short diphenylalanine (FF) peptides modified with 9-fluorenylmethyloxycarbonyl (Fmoc), which promotes the association of the peptide building blocks. Fmoc-FF gels generally form fibrous networks and while other structures have been demonstrated, further control of the gelation and resulting ordered three-dimensional structures potentially offers new possibilities in tissue engineering, sensing, and drug release applications. Herein, we report that the structure tunability of Fmoc-FF gels can be achieved by controlling the water content and the temperature. We further explore the incorporation of metal nanoparticles in the formation of the gel to enable optical sensing applications based on hybrid Fmoc-FF-nanoparticle microspheres. Finally, fluorescence lifetime imaging microscopy reveals a correlation between lifetime and reduced bandgap, in support of a semiconductor-induced charge transfer mechanism that might also increase the stability of an excited state of a probe molecule. The observations potentially further widen the use of these peptide materials in bioimaging and sensing applications.

**KEYWORDS**

Fmoc-FF gels, microspheres, peptide gels, self-assembling nanostructured

## 1 | INTRODUCTION

A specific class of molecular gels that has increasingly attracted the attention of scientists over the past decade are self-assembling materials based on short peptide derivatives. These form ordered fibrous structures, typically based on π–π stacking of β-sheets.[1–7] A widely studied peptide gel is dipeptide fluorenylmethoxycarbonyl-

diphenylalanine (Fmoc-FF), that has been shown to form many different morphologies with nanoscale order.[5–7] The intrinsic hydrophobicity and aromaticity of Fmoc-FF are well-known to promote the hydrophobic and π–π stacking interactions of the fluorenyl rings. Fmoc-FF hydrogels are stable at different temperatures and pH values including acidic conditions.[8] Owing to the ease of chemical modification, low synthesis cost, and biocompatibility,

Fmoc-FF provides opportunities to design materials with unique structural, optical, mechanical, and biological functionalities.[5–7] In turn, these materials have tremendous application potential, often in combination with a second nanomaterial, in a variety of fields, such as cell cultivation,[9] templating,[3] optical devices,[10] catalysis,[4] light harvesting,[11] and wound healing.[12] For example, Erdogan et al.[13] reported a freeze-quenching technique to fabricate plasmonic Au nanorod-embedded porous Fmoc-FF for drug release applications. In addition, Paladini et al.[14] investigated self-assembled Fmoc-FF hydrogel structures loaded with biocompatible, antibacterial Ag nanoparticles (NPs) for wound healing applications.

The formation of spherical micro vesicles has been previously demonstrated and used for drug delivery with other peptides.[15,16] Boc-Phe-Phe-OH dissolved in hexa-fluoro-2-propanol (HFIP) and diluted with ethanol led to the formation of spheres with sizes ranging from 30 nm to 2 μm.[15] In addition, microspheres with diameters ranging from 2 to 3 μm were prepared using Boc-Trp-Leu-Trp-Leu-OMe in ethanol and methanol.[16] In a separate study, Arnon et al.[17] reported that fluorenylmethoxycarbonyl-β,β-diphenyl-Ala-OH (Fmoc-Dip) in ethanol formed needle-like crystals. When the assembly conditions were altered using a "solvent switch" method (i.e., the addition of water to peptide solution prepared in ethanol), spherical particles formed. These spherical particles scattered different wavelengths of light depending on their size (≤2 μm).[17] In these examples, the size of the microspheres did not exceed 3 μm. There is a reported need for larger microspheres that could serve as better carriers for drug delivery.[18] This has motivated us to investigate the possibility of making larger particles from Fmoc-FF by tailoring the sample preparation through solvent and temperature control.

Beyond investigating the role of solvent on the formation of such peptide gels and resultant structures, the effect of temperature is important for several scientific and practical purposes. Some of the applications include fluorescence and Raman based biosensing.[19,20] Despite the fact that peptide-based hydrogel materials have been studied extensively to achieve diverse architectures, including fibrils and ribbons, the role of heating and the interplay with solvent has not been fully explored,[21–23] especially in the presence of metal NPs. Understanding the key factors that control gelation, structure formation, and the functional properties of the resulting gels could potentially open up the use of those materials in new applications.[24–26]

Fmoc-FF gels generally form fibrous networks,[4,27] yet porous microspheres have been demonstrated,[28] and both temperature and solvent have been used to tailor the structure of other peptide-based materials.[28] We have previously reported that bioinspired semiconducting diphenylalanine peptide nanotubes (FFPNTs) can result in structural transition when annealed. Such structures can support Raman detection of $10^{-7}$ M concentrations for a range of molecules, including mononucleotides. The enhancement is attributed to the introduction of electronic states below the conduction band that facilitate charge transfer to the analyte molecule.[29] Thus, in this study, we have investigated the influence of both temperature and water

content on Fmoc-FF gel formation. We have found that microsphere formation can be tuned by increasing the water content and by heating the solution. We further explored the incorporation of metal NPs during gelation to enable optical-based applications, demonstrating the generation of hybrid Fmoc-FF-NP microspheres. Raman, UV–vis, Fourier transform infrared spectroscopy (FTIR), and scanning electron microscopy (SEM) imaging were used to characterize the Fmoc-FF structure. We have also performed computational simulations to study the effect of heat on Fmoc-FF structure. Finally, fluorescence lifetime imaging microscopy (FLIM) was used to provide further insight into the optical properties of Fmoc-FF as a function of heat and water content. The results show that fluorescence lifetime increase with the addition of water. Such results open the possibility of using Fmoc-FF in fluorescent imaging and sensing applications.

## 2 | MATERIALS AND METHODS

All experiments were performed in accordance with the safety guidelines of the University College Dublin Safety, Insurance, Operational Risk and Compliance Office.

### 2.1 | Materials

Diphenylalanine (FF) peptides modified with 9-fluorenylmethyloxycarbonyl Fmoc−FF (B2150, Bachem AG), dimethyl sulfoxide (DMSO) (472301, Sigma-Aldrich), sliver nanoparticles (Ag NPs) (795968, Sigma-Aldrich), Methylene Blue and Crystal Violet (77515, C0775 and Sigma-Aldrich, Ireland).

### 2.2 | Methods

#### 2.2.1 | Fmoc-FF gel preparation

Fmoc−FF hydrogels were prepared using two methods, "solvent switch" and "pH switch." For the "solvent switch" method, Fmoc−FF powder was dissolved in DMSO at a concentration of 100 mg/mL and subsequently diluted in double distilled $H_2O$ (ddH$_2$O) to a final concentration of 2 mg/mL. For the "pH switch" method, Fmoc−FF powder was dissolved in 0.1 M NaOH prepared in ddH$_2$O (no DMSO). The final concentrations of Fmoc-FF used were 1 mg/mL (1:1), 0.5 mg/mL (1:2), 0.25 mg/mL (1:4), and 0.125 mg/mL (1:6).

#### 2.2.2 | Preparation of Fmoc-FF and Fmoc-FF-AgNP templates

Fmoc-FF templates were prepared using 2 mg/mL of Fmoc-FF solution with Ag NPs with a diameter of 40 nm at a concentration of 0.02 mg/mL in water. 200 μL of Ag NP solution was added to 2 mL of the Fmoc-FF with and without heat and left to gel for 4–5 min. The Fmoc-FF solutions

were heated using a hotplate at different temperatures up to 100°C for 5 or 10 min and the temperature of the container was measured using a digital thermometer. The prepared samples were deposited on glass cover slips or Si substrates for further characterization.

### 2.2.3 | Probe molecule solution preparation

Methylene Blue and Crystal Violet were prepared in ddH$_2$O at concentrations of $10^{-5}$ M. The probe molecule solutions were drop cast (40 μL) on the Fmoc-FF and Fmoc-FF-AgNP templates and left to dry for 2–3 h prior to Raman measurements.

### 2.2.4 | Scanning electron microscopy

SEM (JSM-7600F, JEOL, operated at 5 kV) was employed to characterize and observe the location of NPs decorating the surface. The SEM samples were prepared by drop casting on a coverslip or Si substrate. An ~8 nm layer of gold was sputtered on the samples before SEM imaging (Hummer IV, Anatech USA).

### 2.2.5 | Fourier transform infrared spectroscopy

FTIR measurements were performed using Alpha. Platinum-ATR (12209186, Bruker). A small drop of FF-PNT (10 μL) was placed on the ATR diamond crystal. The spectrum was collected using transmission mode, scanning from 1400 to 4000 nm.

### 2.2.6 | UV–Vis absorbance spectrometry

Optical absorbance measurements of FF-PNTs with and without Ag NPs were performed on an UV–Vis absorbance spectrometer (V-650, JASCO, Inc.) under identical settings: 1 nm step size, 1 nm bandwidth, and 400 nm/min scan speed across a 190–900 nm range. A quartz cuvette or glass cover slip was used to conduct the measurements. A standard 1 cm (in path length) cuvette cell was used.

### 2.2.7 | Raman spectroscopy

Raman and photoluminescence (PL) measurements were performed using a bespoke Raman system that consisted of an inverted optical microscope (IX71, Olympus), a monochromatic laser (HeNe, ThorLabs) with a beam splitter and a long pass filter (RazorEdge, Semrock), a spectrograph (SP-2300i, Princeton Instruments), and a CCD camera (IXON, Andor). To focus on the laser (532 nm wavelength, 5 mW incident power), a 50× objective was used. Raman and PL spectra were collected with an exposure time

of 1 s. An average of typically 10 measurements was reported. Toluene was used for calibration of the Raman and PL signal over the spectral window.

The SERS enhancement factor was calculated as ($N_{vol}$ * $I_{SERS}$)/($N_{surf}$ * $I_{Raman}$), where $N_{vol}$ and $N_{surf}$ are the number of molecules probed in the sample and on the SERS substrates, respectively, and $I_{SERS}$ and $I_{Raman}$ are the SERS and Raman intensities. Assuming the number of molecules is the same on the substrate, as we are using the same volume, both $I_{SERS}$ and $I_{Raman}$ are peak to peak intensity. Therefore, the baselines were subtracted from the initial peak intensities.

### 2.2.8 | Fluorescence imaging

Fluorescence images were recorded using a fluorescence microscope (Zeiss AxioImager M1), with 20× and 50× objectives, an exposure time of 10 ms, and excitation wavelengths of 300, 500, and 600 nm.

### 2.2.9 | Fluorescence lifetime imaging microscopy

Fluorescence confocal and fluorescence lifetime imaging microscopy images were obtained with a Leica TCS SP8 confocal system using a 532 nm excitation wavelength and an internal HyD GaAsP SMD detector. Fitting of FLIM data was performed using FLIMfit 5.1.1. A 10× objective was used and the samples were imaged through a coverslip in air, without the introduction of a mounting medium.

### 2.2.10 | Theoretical calculations

The corresponding molecular structure was fully optimized using Density Function Theory (DFT) as implemented in the QuantumATK software[30] using a local combination of the atomic orbitals (LCAO) approach, the Perdew, Burke, Ernzerhof (PBE) functionals,[31] the norm-conserving PseudoDojo[32] pseudopotential with medium basis set, and a mesh cut-off energy of $10^5$ Ha. The calculation of the self-consistent field (SCF) considered a tolerance limit of $10^{-6}$ Ha for energy convergence. The geometry structure and ion relaxations were performed using the limited-memory Broyden–Fletcher–Goldfarb–Shanno (LBFGS) algorithm, including the force on each atom less than 0.05 eV/Å. In addition, a molecular dynamics simulation, based on heating runs through a simulated annealing protocol, is conducted using the reactive force field (ReaxFF) at temperatures of 100°C. NVT *Nose Hoover* algorithm[30] was used in the calculations, which has a 1 fs calculation time step along with 100 fs of thermostat timescale. The reservoir temperature, which specifies the temperature of the heat bath, is kept at 100°C. At the study temperature, the starting velocities of the atoms follow the Maxwell–Boltzmann distribution. Water molecules were not included in the calculation.

# 3 | RESULTS AND DISCUSSION

In this work, we have investigated the influence of increasing $ddH_2O$ content and temperature on Fmoc-FF hydrogel formation using widely used[4,33] "pH switch" (Figures 1 and 2 and Figure S1) and "solvent switch" (Figure S2) methods, initially without and subsequently with Ag NPs. The "solvent switch" method relies on the addition of $ddH2O$ water to a stock peptide solution (100 mg/mL) prepared in an organic solvent (DMSO).[5] The $ddH_2O$ water has lower solubility, triggering spontaneous self-assembly into an organized structure. The peptide backbones form hydrogen bonds necessary to create β-sheets, while the aromatic nature of the fluorenyl group and the amino acid side groups allow for π–π stacking interactions, which are highly anisotropic and short-range relative to the size of the Fmoc-FF molecule.[3–5,24] In the "pH switch" method, gel formation is achieved by lowering the initial pH of the peptide solution (pH = 10.5) with the progressive addition of HCl.[4] Studies have demonstrated that Fmoc-FF can assemble in a β-sheet structure when prepared via "pH switch."[4,24] For the titration experiment with $ddH_2O$, Fmoc-FF was mixed with $ddH_2O$ at different ratios from 1:1 to 1:6.

## 3.1 | Role of water content

An SEM image of a Fmoc-FF gel prepared using "pH switch" is shown in Figure 1a. Following the formation of the gel, different Fmoc-FF to $ddH_2O$ ratios from 1:1 to 1:6 were investigated by SEM

(Figure 1b–d). The diameters (widths) of the fibrils were determined to increase with increasing water content from 0.3 ± 0.1 μm (1:1) to 0.4 ± 0.1 μm (1:4) and 0.5 ± 0.1 μm (1:6) (Figure S3) from measurements of more than $n = 30$ fibrils in each case. Notably, with the addition of water, "pH switch" resulted in the formation of microsphere structures that increased in size with increasing water content. The diameters of the microspheres were determined to be 0.22 ± 0.03 μm (1:1), 0.4 ± 0.1 μm (1:4), and 0.6 ± 0.2 μm (1:6) (Figure S3) from measurements of more than $n = 30$ fibrils in each case.

Typically, Fmoc-FF self-assembles into a nanofibrillar hydrogel in $ddH_2O$ via hydrogen bonding and π–π interactions, leading to the formation of β-sheet structures.[1–4,34] The addition of water to Fmoc-FF leads to the formation of larger β-sheet structures and therefore larger fibrils, in agreement with previous reports.[1–5,34] Ordered fibrils were produced when the Fmoc-FF was prepared via "solvent switch" (Figure S2); however, increasing the $ddH_2O$ content did not result in microsphere formation, indicating that the pH adjustment plays a significant role in microsphere formation. The final Fmoc-FF concentration after the addition of $ddH_2O$ is shown for both methods in Table S1.

To further understand the influence of $ddH_2O$ content on the resulting structures, FTIR, UV–vis, and Raman measurements were undertaken (Figure 1e–g). FTIR measurements of Fmoc-FF prepared using "pH switch" (Figure 1e) revealed appreciable changes in bands located at 3232, 3354, and 3674 $cm^{-1}$, corresponding to O—H, N—H, and C—H stretching vibrations, respectively, upon the addition of $ddH_2O$. Ziganshin et al.[19] previously associated a red shift of N—H
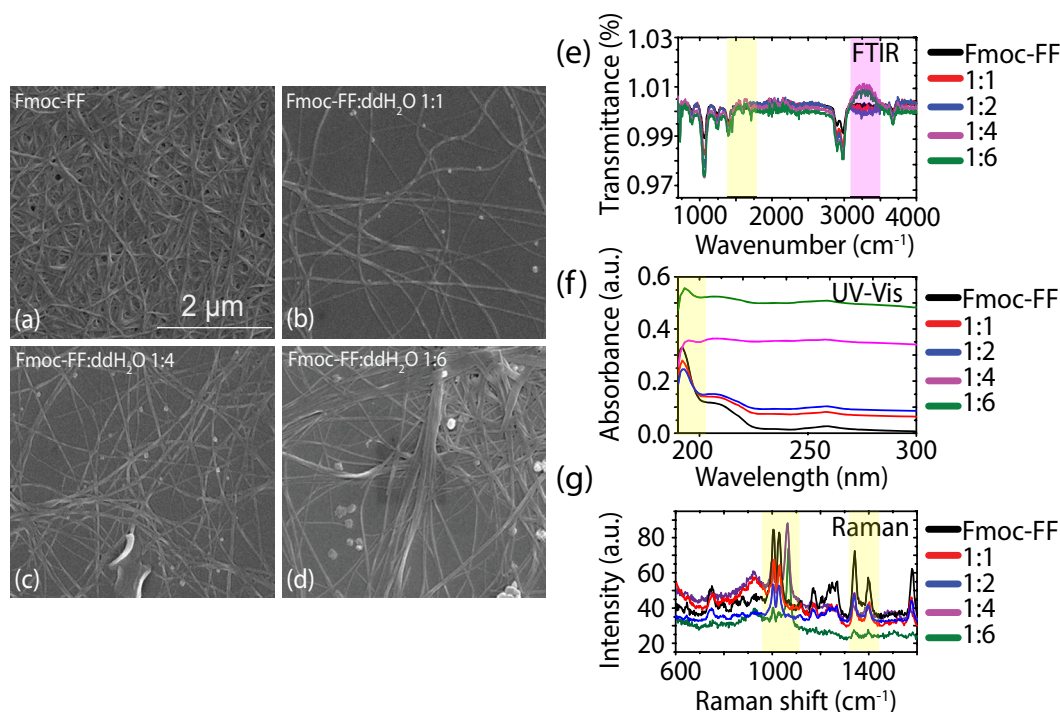


**FIGURE 1**  Role of water content on the formation of Fmoc-FF gels prepared using the "pH switch" method. (a–d) SEM images of Fmoc-FF gels prepared with different Fmoc-FF:$ddH_2O$ ratios (1:1–1:6). (e) FTIR, (f) UV–vis, and (g) Raman data of Fmoc-FF gels prepared with different Fmoc-FF:$ddH_2O$ ratios (1:1–1:6).
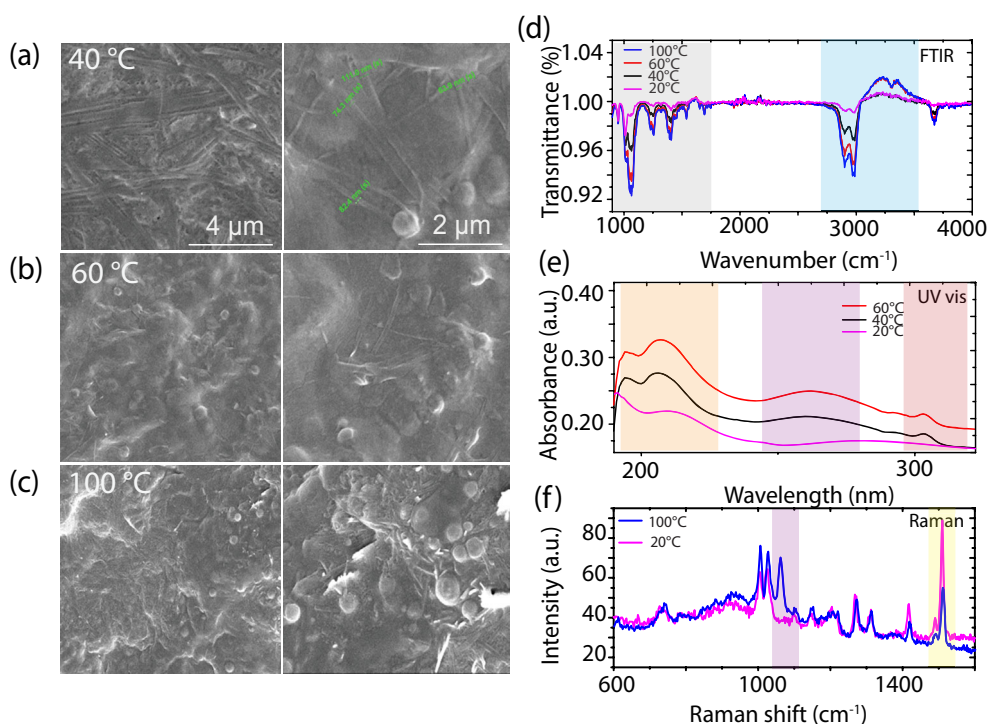
**FIGURE 2** Role of temperature on Fmoc-FF formation prepared using the "pH switch" method. (a–c) SEM images and (d) FTIR, (e) UV–vis, and (f) Raman measurements of Fmoc-FF at 20–100°C. The regions highlighted in (d–f) indicate where the most significant changes occurred.

stretching upon heating dipeptides to the formation of additional hydrogen bonds associated with the N—H group. Bands at $1633 \text{ cm}^{-1}$, consistent with the presence of β-sheet structures, and $1653 \text{ cm}^{-1}$, characteristic of parallel arrangement of the β-sheets, both associated with Fmoc-FF fibril formation, were present.[1–3,34] Bands associated with parallel β-sheets[15,16] such as $1536 \text{ cm}^{-1}$ (amide II N—H bending) and $1690 \text{ cm}^{-1}$ (amide I carbonyl C═O stretching) were observed (Figure 2d and Figure S2e). Other studies have shown that parallel β-sheet structures in FF-based (i.e., Boc-Phe-Phe-OH) microspheres form through the creation of a network of hydrogen bonds and π–π interactions, whereby the carbonyl groups at $\sim1693 \text{ cm}^{-1}$ result in the formation of a spherical structure.[35,36] FTIR spectra remained largely unchanged when Fmoc-FF was prepared via "solvent switch." All band assignments were in agreement with literature reports for Fmoc-FF in fibrillar form (Figure S2e).[4,5,24]

UV–vis spectra for Fmoc-FF prepared using "pH switch" and "solvent switch" methods as a function of $ddH_2O$ content are shown in Figure 1f and Figure S2f. Fmoc-FF prepared using both methods exhibited a peak at the long-wavelength edge (314 nm), in line with literature reports.[1–3] With the addition of water to Fmoc-FF prepared using "pH switch," the absorption increased and with high water content (1:4 and 1:6). The UV–vis spectra lose their structure and become flat. The bandgap was determined from UV–vis data following previous reports[37,38] to decrease from 4.8 ± 0.1 (control samples) to 3.9 ± 0.1 eV at 1:6 ratio. Studies have shown that the presence or addition of $ddH_2O$ leads to changes in the electronic properties of peptide-based materials that reduce the bandgap and

lead to increased conductivity.[39] The increased conductivity could be associated with the alignment of the $ddH_2O$ molecules' dipole moments that results in a larger dipole moment of the overall structure.[39] Fmoc-FF prepared using "solvent switch" experienced only slight changes in absorption and a smaller decrease in the calculated bandgap from 4.6 ± 0.1 to 4.1 ± 0.1 eV (Figure S2f). This observation suggests that Fmoc-FF prepared using "pH switch" is more sensitive to changes in the $ddH_2O$ content.

Raman spectra for Fmoc-FF prepared using both methods as a function of $ddH_2O$ content are shown in Figure 1g and Figure S2g. Raman bands for Fmoc-FF prepared using "pH switch" were more apparent (Figure 1g) in comparison to Fmoc-FF prepared using "solvent switch" where DMSO bands (682 and $713 \text{ cm}^{-1}$) dominated the spectra (Figure S2g). Raman of Fmoc-FF prepared using "pH switch" presents the typical breathing modes at 998 and $1020 \text{ cm}^{-1}$ and other characteristic bands (719, 736, 1265, 1350, 1412, 1452, and $1507 \text{ cm}^{-1}$) all in agreement with the literature reports.[3] As the water content increased, bands associated with Fmoc-FF, such as the aforementioned breathing modes, decreased in intensity, as expected. A new sharp band formed at around $1160 \text{ cm}^{-1}$ (C—H stretching) that could be an indication of microsphere formation (Figure 1g).

## 3.2 | Role of temperature

Studies have shown that hydrophobic interactions are enhanced while hydrogen bonding interactions are weakened with increasing

temperature.[40] Given the role of hydrophobic interactions and hydrogen bonding on the self-assembly of peptides, and as evidenced above for Fmoc-FF in particular, we next investigated the effect of heating on Fmoc-FF prepared using "pH switch" (with no changes in water content) at 20–100°C for 5 min in closed containers. During self-assembly, Fmoc-FF molecules form cylindrical nanofibrils by interlocking four twisted antiparallel β-sheets through lateral antiparallel π–π interactions,[9] as shown in Figure 2a. Scanning electron microscope (SEM) images of Fmoc-FF prepared via "pH switch" as a function of temperature are shown in Figure 2a–c. At 20°C, Fmoc-FF exhibited a dense network of fibrous structures with diameters of 102 ± 43 nm ($n = 30$ fibrils), in line with literature reports.[3] As the temperature increased, the microspheres formed and increased in diameter, as shown in Figure S4. The diameter was 1.0 ± 0.3 μm at 40°C, 1.1 ± 0.2 μm at 60°C, and 1.2 ± 0.3 μm at 100°C. Not only do microspheres form after 5 min of heating at 100°C, but they also form when heating at 50°C for 10 min when using Fmoc-FF prepared by "pH switch" (Figure S5). When using "solvent switch," no microspheres were observed at any temperature; only slightly increased fibril diameters were observed (up to 120 ± 65 nm [$n = 30$ fibrils]) at 100°C (Figure S6).

Fmoc-FF samples prepared at different temperatures were further analyzed by FTIR, UV–vis, and Raman spectroscopy, as illustrated in Figure 2d–f. The FTIR spectrum of Fmoc-FF prepared using "pH switch" (Figure 2d and Figure S7) at 20°C (Figure S4a) has weak amide I bands in the range 1500–1600 cm$^{-1}$, similar to the band assignments reported in Figure 1f. However, more intense bands started to appear with increasing temperature, such as the band at 1539 cm$^{-1}$ associated with N—H bending (amide II), other amide II bands at 1693 and 1746 cm$^{-1}$, and the band at 1746 cm$^{-1}$ attributed to C═O stretching.[5] The red shift and split of the N—H stretching band at 3223 and 3354 cm$^{-1}$ after heating to 100°C might indicate a rearrangement of hydrogen bonds.[19] All bands between 3000 and 3500 cm$^{-1}$ are attributed to O—H, N—H, and C—H, as described previously.[19] No significant changes were observed in FTIR measurements when Fmoc-FF was prepared via "solvent switch" at different temperatures.

UV–vis spectroscopic analysis of Fmoc-FF prepared using "pH switch" and "solvent switch" methods as a function of temperature is shown in Figure 2e and Figure S6f. From both methods, there was a slight increase in the absorption intensity with temperature compared to Fmoc-FF (Figure 1g). When using "pH switch" at 100°C, the UV–vis spectrum becomes flat in around 200–220 nm. There was an increase in the bands at 260 nm (as shaded in purple in Figure 2e) and a blue shift in bands located at 320 nm. These changes were not present when Fmoc-FF was prepared via "solvent switch," suggesting that "pH switch" is more sensitive to temperature. The bandgap was determined from UV–vis data to have decreased from 4.8 ± 0.1 eV at 20°C to 4.6 ± 0.1 eV at 60°C, and to 4.1 ± 0.2 eV at 100°C for "pH switch." From this observation, we have concluded that Fmoc-FF prepared by the pH switch method is more sensitive to temperature changes; however, further studies are needed to fully understand the underlying mechanism.

## 3.3 | Computational simulations of the effect of heat

To gain an in-depth understanding of the effect of heating on the Fmoc-FF molecular structure (Figure 3a and Figure S8), we investigated its structural evolution using computational simulations. The molecular packing models were constructed based on three parallel stacks of Fmoc-FF molecules along the crystallographic y-axis to account for the formation of extended structure (Figure 3b). Hydrogen bonding and weak offset π–π interactions corresponded to a distance of 5.0 Å and are evident between these Fmoc-FF molecule
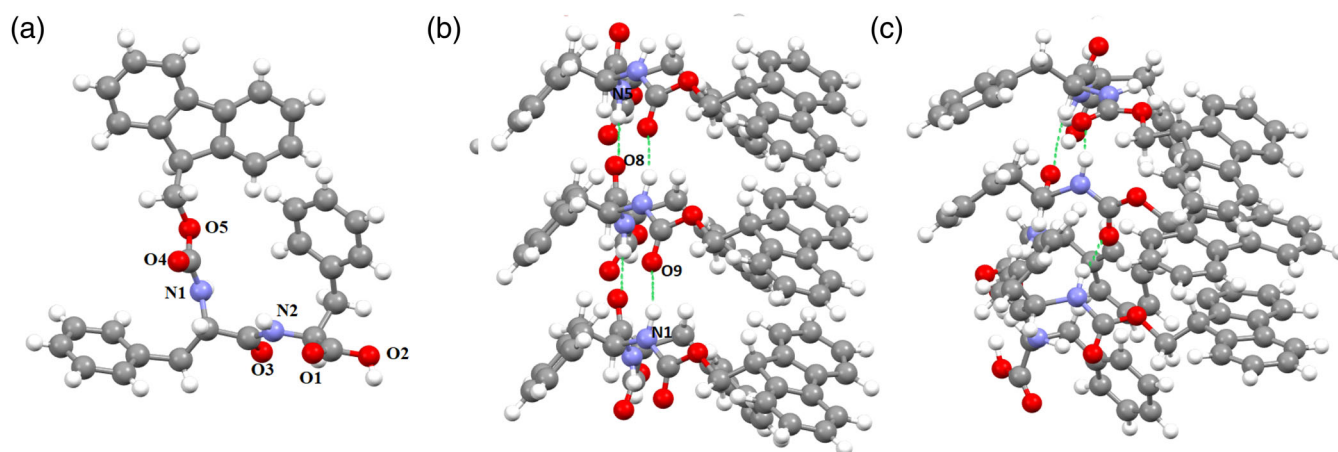


**FIGURE 3** Computational simulations of Fmoc-FF structure. (a) The optimized molecular structure of an Fmoc-FF molecule, showing the atom-labelling scheme. Side-by-side stacking through amide hydrogen bonds along the y-axis (b) before and (c) after heating at 100°C. The gray, blue, red, and white balls indicate C, N, O, and H atoms, respectively. The inter-molecular hydrogen bonds are highlighted in green.

sheets. Figure 3b shows the optimized hydrogen-bonding network structure, while the bond lengths and angles of the hydrogen bonds are presented in Table S2. It is observed from the plots that the molecular packing is described by intra- and intermolecular hydrogen bonds characterized by different functional groups present in the structure (—CO, —COOH, —O—, —NH). HN(1) and HN(5) form intermolecular hydrogen bonds to O(9) and O(8) atoms in a carbonyl group of an adjacent molecule, respectively, that stabilize the molecular sheet structure along the y-axis (see Figure 3b).

A molecular dynamics simulation, based on heating runs through a simulated annealing protocol, is carried out at temperatures of 100°C, lasting for 5 ps with a time step of 1 fs. As illustrated in Figure S9, the potential energy of the Fmoc-FF system varies around a constant value of −1204 eV with a considerably small fluctuation magnitude, showing the thermal stability of the newly obtained structure. The fully relaxed structure after 5 ps at 100°C is plotted in Figure 3c, where geometry reconstruction occurs, demonstrating a deformation of the stacked arrangement of Fmoc-FF sheets during the temporal evolution. Moreover, aromatic π−π stackings were reduced for two Fmoc-FF sheets with centroid distances of 3.309 Å. The molecular sheet structure after heating shows pronounced deformations via rotations of the different hydrophobic side groups (e.g., C19—O5—C20—C21 torsion angle has a larger deviation than that of the molecular structure before heating, see Table S3). These results are consistent with our experimental measurements. Water molecules were not included in the simulation.

## 3.4 | Influence of the presence of Ag NPs

In order to understand the influence of the presence of Ag NPs, which would normally widen the use of Fmoc-FF in optical sensing

applications,[4,8] Ag NPs were incorporated within the structures. Adding NPs to Fmoc-FF gels prepared using "solvent switch" (Figure S10) yields results in line with literature reports.[3]

SEM images of Fmoc-FF prepared by "pH switch" in the presence of Ag NPs (Figure 4a) revealed fibrils with a typical diameter of 83 ± 15 nm; however, when heated at 100°C, the fibrils formed a microsphere-like structure that encapsulated the fibers (Figure 4b). The small fibers assembled into thick fiber bundles and formed more densely packed and entangled three-dimensional networks. However, upon cooling after heating the solution, the encapsulated fibers start to spread again over the surface upon drying, highlighting the reversibility of the process (Figure S11).

To understand the influence of NPs on gel formation and optical properties, FTIR, UV–vis, and Raman investigations were undertaken. FTIR data (Figure S12) are comparable to those in Figure 2, revealing the appearance of strong amide I bands located at ~1690 and ~1650 cm$^{-1}$ (C=O), an amide II band at ~1530 cm$^{-1}$ (N—H), as well as O—H stretching at 3227 cm$^{-1}$ and N—H stretching at 3367 cm$^{-1}$ bands.

From UV–vis data, it was determined that the bandgap decreased from 4.6 ± 0.1 eV at 20°C to 3.8 ± 0.2 eV at 100°C, slightly lower than in the absence of the Ag NPs. In addition, a broadening and red shift (~20 nm) of the surface plasmon resonance (SPR) of Ag NPs (at 420 nm) was observed (Figure 4f).[5] Tuning the SPR of NPs, as demonstrated here, is of interest for optical and bio sensing applications.

Heat plays a significant role in the gel formation, as Raman data show changes including increased Raman intensity with increasing temperature in gels prepared using both methods (Figure 4g and Figure S11d). Raman spectra of DMSO, pure Fmoc-FF, and "solvent switch" Fmoc-FF heated at different temperatures ranging from 20 to
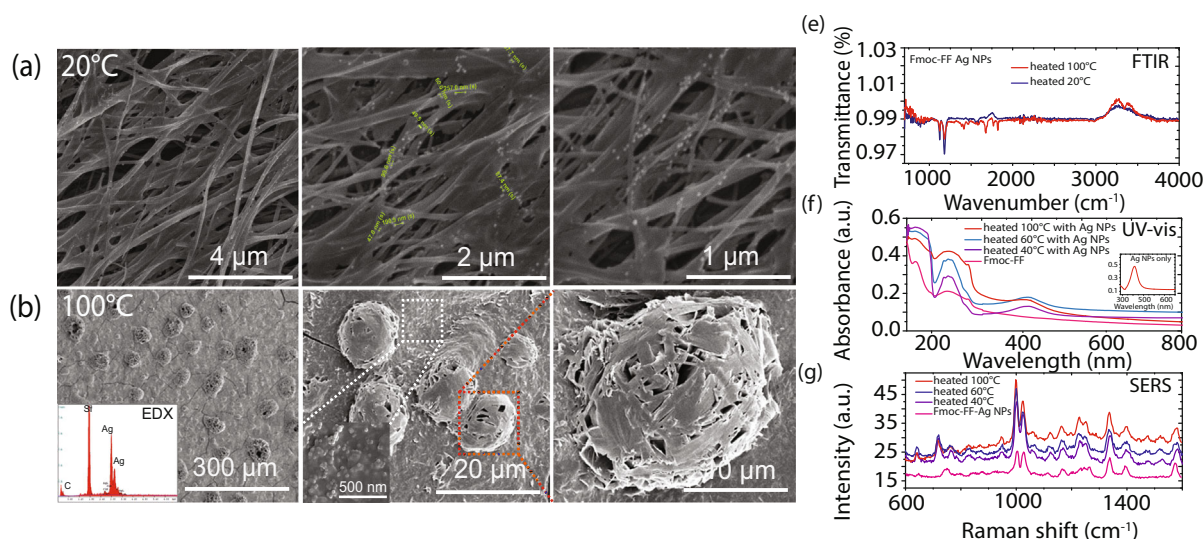


**FIGURE 4** Role of temperature on Fmoc-FF-AgNP composites, prepared using the "pH switch" method. SEM images of Fmoc-FF with Ag NPs at (a) 20°C and at (b) 100°C. (e) FTIR measurement of Fmoc-FF with Ag NPs at a different temperature. (f and g) UV–vis and surface enhanced Raman (SERS) measurements of Fmoc-FF at a different temperature, respectively. The inset in (f) shows the absorption spectra of Ag NPs with SPR located at 420 nm.
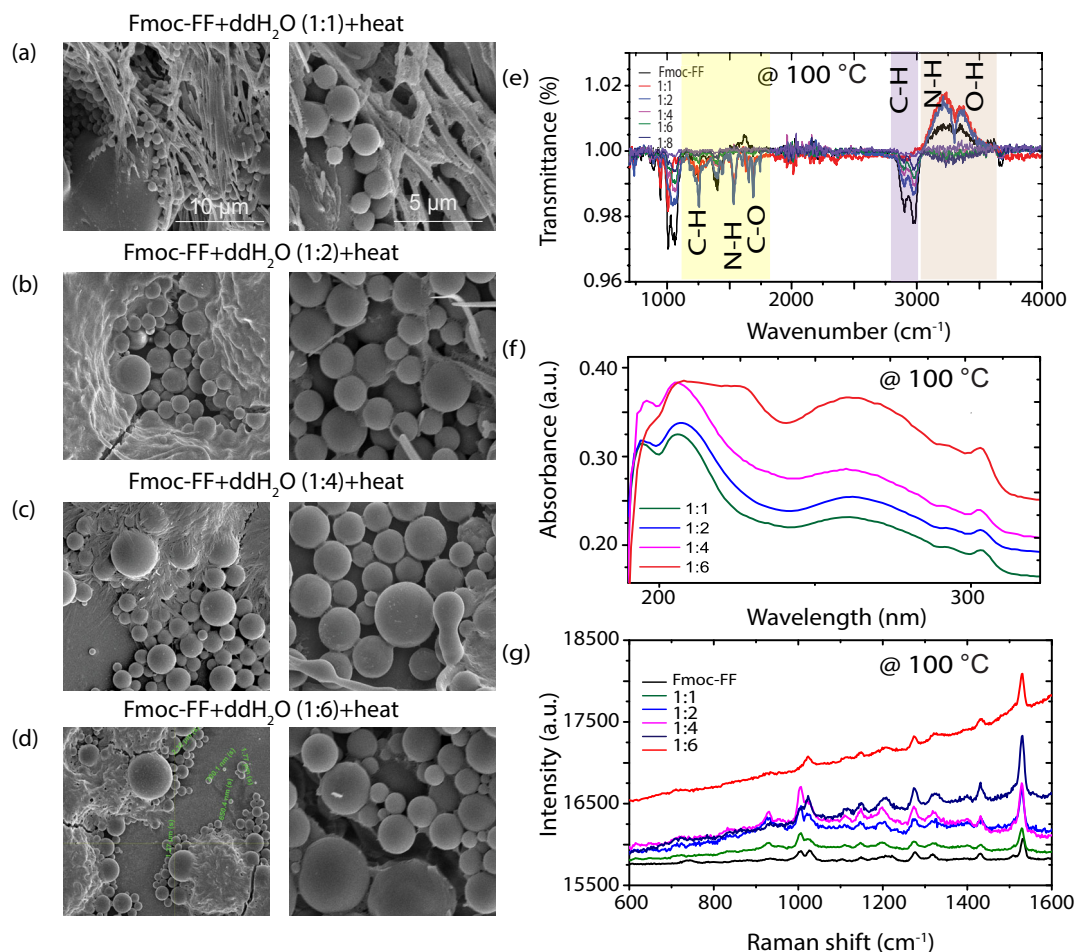
**FIGURE 5** Role of water content on microsphere size of Fmoc-FF prepared at 100°C using the "pH switch" method. (a–d) SEM images of Fmoc-FF prepared using "pH switch" with different water ratios in the absence of Ag NPs. (e) FTIR, (f) UV–vis, and (g) Raman data for Fmoc-FF prepared at 100°C with different water ratios.

100°C are shown in Figure S6g (in the absence of Ag NPs). Without heat, only bands from DMSO were detected, such as bands at 680 and 720 cm$^{-1}$. Upon heating, bands such as ring breathing modes at 1000 and 1050 cm$^{-1}$ appeared that are attributed to Fmoc-FF (Figure S6). On the other hand, using "pH switch" to prepare the Fmoc-FF, new sharp bands started to form at around 1160 cm$^{-1}$ (C—H stretching) that could be an indication of microsphere formation. When Ag NPs were mixed with Fmoc-FF (Figure 4g) almost all Fmoc-FF bands were detectable with ∼7-fold increase in intensity in comparison to Fmoc-FF alone.

## 3.5 | Effect of increasing water content at a fixed temperature of 100°C

Given that hydrophobic interactions and hydrogen bonds are key to the formation and stability of secondary structure of peptides, they can be affected by temperature.[40] We have investigated the effect of both heat and water content on Fmoc-FF prepared only by "pH switch" as "solvent switch" did not produce spherical structures.

Interestingly, combining heating at 100°C and titration experiments (e.g., 1:1 ratio) without and with NPs (Figures 5 and 6) resulted in the transformation of most of the fibrils to spherical structures with a range of nanometer to micrometer sized diameters, as illustrated in the histograms shown in Figures S13 and S14. At 100°C, the diameter was 1.6 ± 0.4 μm at 1:1 ratio with ddH$_2$O, 2.6 ± 0.7 μm at 1:2, 3.1 ± 1.0 μm at 1:4, and 4.2 ± 1.8 μm at 1:6.

As before, the FTIR spectrum of the heated Fmoc-FF (Figure 5e) showed additional bands, for example, at 1633 and 1534 cm$^{-1}$ assigned to C=O stretching (amide I) and N—H bending (amide II) band, respectively. The position of the amide I band at 1633 is red shifted to ∼1653 cm$^{-1}$ upon the addition of ddH$_2$O at 100°C. From the UV–vis data (Figure 5f), a significant reduction in the bandgap was calculated from 4.6 ± 0.1 eV at 20°C to 3.3 ± 0.1 eV at 100°C (in the absence of NPs) and further to 3.1 ± 0.1 eV (in the presence of NPs) for a ratio of 1:6. In this work, the tuneability of the bandgap has been demonstrated to extend from 3.1 to 4.8 eV for Fmoc-FF based structures.

To distinguish the dominant Raman and FTIR bands of fibrils and microspheres, they were centrifuged in the presence and absence of Ag NPs (Figure 6). The opaque part (referred to as bottom in the inset
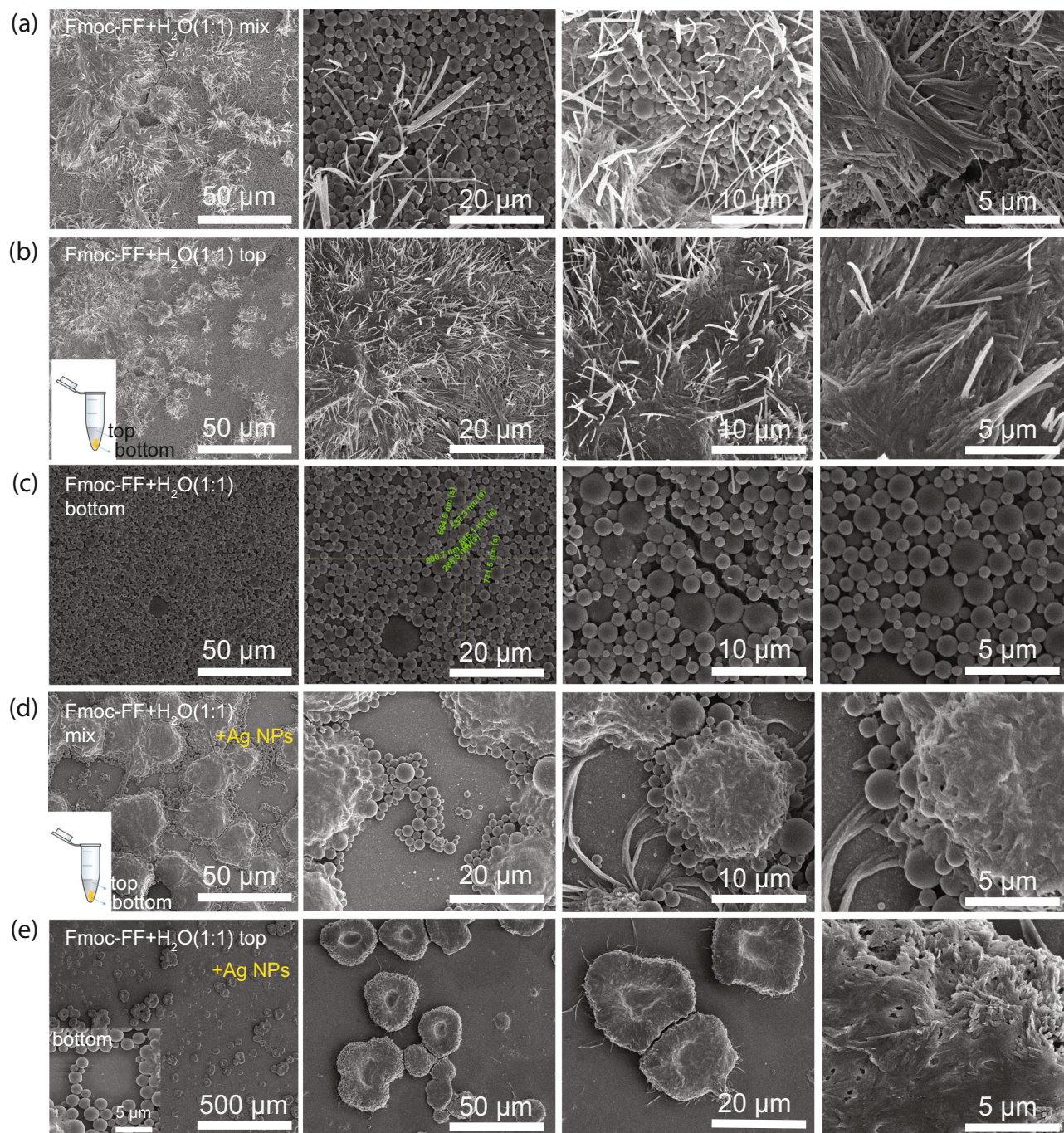
**FIGURE 6** Separation of microspheres from fibrils by centrifuge of Fmoc-FF prepared using the "pH switch" method. (a–e) SEM images of Fmoc-FF:ddH₂O 1:1 heated at 100°C (a–c) without Ag NPs and (d–e) with Ag NPs. The insets in (b and d) illustrate the separation of Fmoc-FF microspheres. The inset in (e) shows microspheres prepared with Ag NPs.

of Figure 6) primarily contained microspheres of various sizes, reaching up to several micrometers in diameter. The transparent solution (top in the inset of Figure 6) primarily contained fibrils, however, when Ag NPs were included, enclosed donut-shaped fibril aggregates with an average diameter of 47.2 ± 12.4 μm were present (Figure 6e). A comparison of Fmoc-FF microspheres formed using "pH switch" and literature reports of peptide microspheres is shown in Table S4.

FTIR, PL, UV–vis, and Raman were used for the characterization of Fmoc-FF after centrifuge and separation with and without Ag NPs to distinguish and precisely determine the optical features of microspheres and fibrils (Figure 7 [FTIR, PL, Raman], Figures S15 [FTIR], and S16 [UV–vis]).

The FTIR spectrum after Separation (Figure 7a,b and Figure S15) provided more insight in the assignment of features associated with
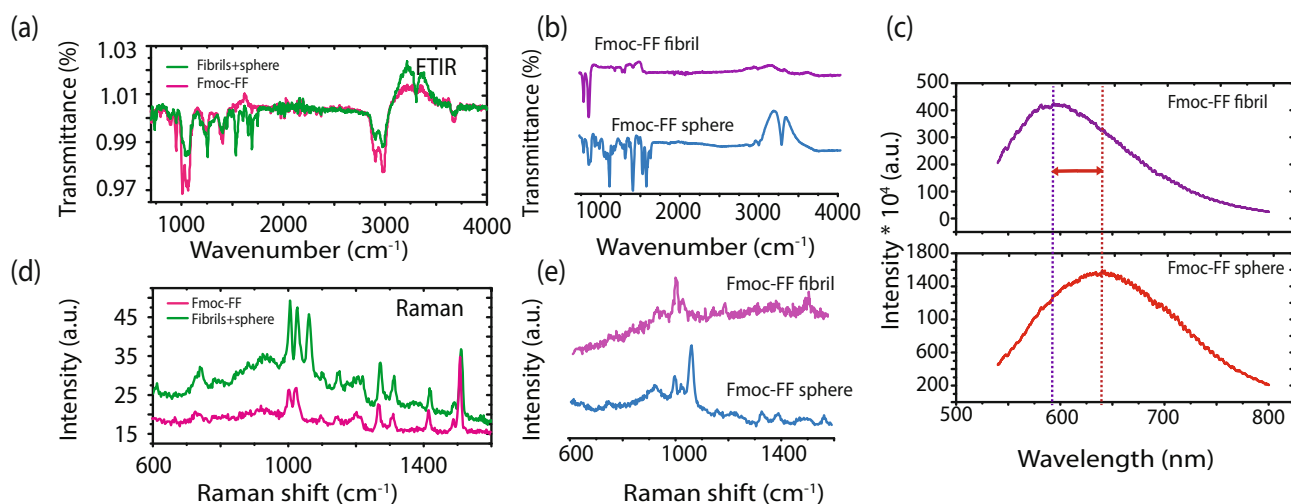
**FIGURE 7**  Optical characterization of the fibrils and microspheres from Fmoc-FF prepared using the "pH switch" method after centrifuge separation. (a, b) FTIR, (c) PL, and (d, e) Raman data for Fmoc-FF (1:1) heated at 100°C.

each phase. It can be seen in Figure 7a,b, when comparing the FTIR spectra of the fibrils versus the microspheres that the microspheres have the most dominant bands. Additionally, bands located at 1253, 1536, and 1650 cm$^{-1}$ are more pronounced in the microspheres. Fmoc-FF fibrils (location 2 in Figure S15b) show the predominant antiparallel β-sheet character based on the position of the amide I band, as described earlier (Figure 1). However, microspheres (location 1 in Figure S15b), reveal a parallel β-sheet mode with the amide I band from at 1633 cm$^{-1}$ red shifted to ~1650 cm$^{-1}$ (C=O stretching, amide I). There was a red shift of other bands, for example, 1006–1008 cm$^{-1}$, and an increased intensity of bands between 1137 and 1536 cm$^{-1}$, as shown in Figure 7a,b. The peaks corresponding to antiparallel β-sheet structures are still observed, but their intensity is weaker. Additional peaks are observed in the amide II region at 1693 and 1744 cm$^{-1}$. The peak at 1693 cm$^{-1}$ has been assigned in the literature to peptides adopting a sphere shape.[21,22] The findings suggest that Fmoc-FF loses its antiparallel β-sheet organization to form microspheres with a predominant parallel β-sheet structure. The exact nature of the induced structure, however, has not been yet elucidated.

To get information about the optical features of Fmoc-FF after separation, PL (Figure 7c) was used to determine the emission spectra of fibrils and microspheres. The fibril emission peak at 598 nm shifts to 655 nm for the microspheres. The PL peak at 655 nm, under excitation at 532 nm, has an intensity 10 times higher than the intensity of the 598 nm peak under the same excitation, highlighting the microspheres as promising materials for bioimaging and sensing (Figure S17).

Differences in Raman spectra between Fmoc-FF and a sample containing both fibrils and spheres (Figure 7d) as well as between separated spheres and fibrils (Figure 7e) are apparent. Raman spectra show a sharp new band forming at around 1160 cm$^{-1}$ (C-H stretching), similar to data in Figure 1g.

Separation by centrifuge was also performed on Fmoc-FF prepared with AgNPs. Surface enhanced Raman spectroscopy (SERS) measurements of Fmoc-FF-AgNP structures before and after the separation of fibrils and microspheres are shown in Figure S18. Two probe molecules, Crystal Violet and Methylene Blue, at concentrations of 10$^{-5}$ M, were investigated. The highest SERS intensities were observed for Fmoc-FF-AgNP prepared with ddH$_2$O (1:1) and heated at 100°C. Notably, in the presence of microspheres, both SERS and fluorescence background increase. A 7–8-fold SERS enhancement is observed (Figure S18c,f). The enhancement can be attributed to the electromagnetic enhancement resulting from the presence of Ag NPs, but charge transfer and changes in band structure likely contribute.[41] The results highlight the potential for using the microspheres in SERS sensing applications and a potential avenue to explore charge transfer via hydrogen bond-tuning.[41] Not only was an enhancement in SERS intensity observed but also an increase in PL signal was seen. Figure S19 shows emission spectra of CV and MB on pristine and annealed Fmoc-FF at 100°C with and without water content and with and without Ag NPs. It can be seen from both molecules used that the highest PL intensity was recorded when using Fmoc-FF spheres at 1:1 water ratio at 100°C with Ag NPs. Both the addition of water and heat result in increased PL intensity in comparison to control samples when using CV or MB on cover slips, for instance, or when using Fmoc-FF only without further treatment, resulting in a 16-fold increase with NP and a 7-fold increase without NPs in PL for MB on Fmoc-FF spheres at 1:1 ratio with water and 100°C (Figure S19c,d). The increase in PL intensity could be attributed to the fact that both heat and water change the hydrophobic interactions and hydrogen bonding, affecting intermolecular interaction and hence enhancing the PL intensity.[38,42] Similar results were observed when using CV (Figure S19).

To better understand the Raman enhancement mechanism, fluorescence lifetime imaging microscopy (FLIM) by multidimensional time-correlated single-photon counting was performed (Figure 8). In
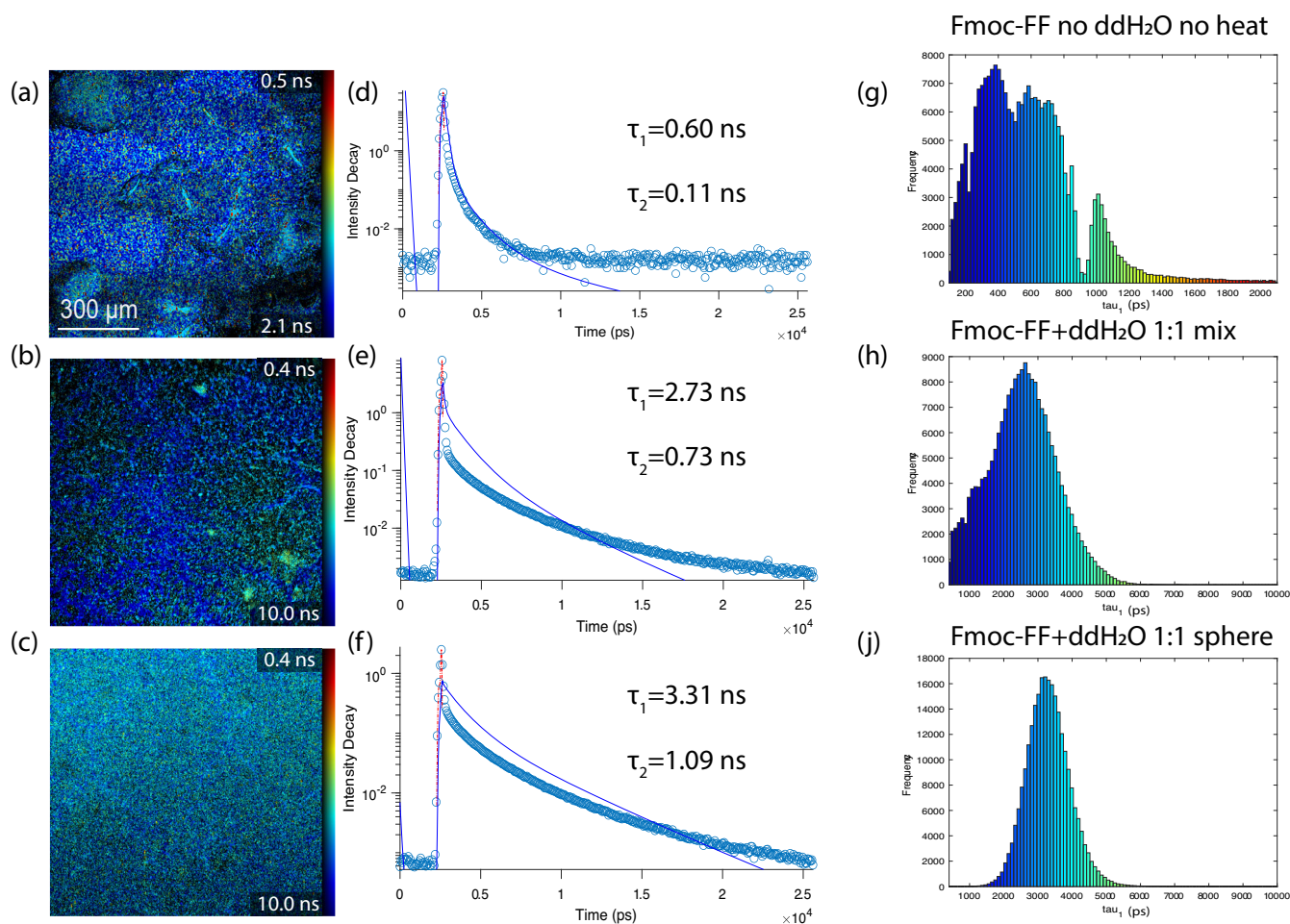
**FIGURE 8** Fluorescence lifetime imaging microscopy of Fmoc-FF prepared using the "pH switch" method. (a, d, g) Fmoc-FF control without the addition of water or heat, (b, e, h) Fmoc-FF (1:1) at 100°C, and (c, f, j) centrifuged Fmoc-FF (1:1) microspheres at 100°C. (a–c) Fluorescence images. (d–f) Fluorescence decay curves (circles are experimental data points and continuous lines are the fitting curves) along with the fitted lifetimes. (g–j) Histograms of the fitted $\tau_1$ lifetimes.

the absence of probe molecules, the fluorescence lifetimes for Fmoc-FF increased from $\tau_1 = 0.60$ ns and $\tau_2 = 0.11$ ns without the addition of ddH$_2$O and no heating to $\tau_1 = 3.31$ ns and $\tau_2 = 1.09$ ns for Fmoc-FF microspheres prepared at 100°C with 1:1 ddH$_2$O. Thus, increased lifetimes are correlated with the decreased bandgap observed and suggest a charge transfer mechanism that might also increase the stability of an excited state of a probe molecule. FLIM of TMPyP on Fmoc-FF prepared by "pH switch" (Figure S20) reveals that the fluorescence lifetime increased from $\tau_1 = 3.80$ ns and $\tau_2 = 0.95$ ns when the uncentrifuged Fmoc-FF was prepared at 20°C to $\tau_1 = 5.15$ ns and $\tau_2 = 0.94$ ns on centrifuged Fmoc-FF microspheres prepared at 100°C. The observed increase in a lifetime could be due to a semiconductor-induced charge transfer process, allowing extended lifetime for the excited singlet state between Fmoc-FF and TMPyP.[43] Our findings are in agreement with previous studies[38] reporting that charge transfer from peptide-based materials can stabilize the excited state of the photosensitizer or dye molecules.

The formation of FF fibrils, nanotubes, and nanospheres by aromatic dipeptides is facilitated by the closure of two-dimensional peptide layers.[44] Previous reports have shown that solvent composition and overall solution conditions are strong determinants of the supramolecular nanostructure morphology of Fmoc-FF. In this work, we show Fmoc-FF could form either fibrils or spherical structures upon heat and changing the water ratio, both of which can affect hydrogen bonding and hydrophobic interactions that can alter the peptide self-assembly. Given the expectation that hydrogen bonding is weakened with temperature whereas hydrophobic interactions are enhanced, it is expected that this interplay is key to the fibril-to-sphere transition. Further work is needed, however, to understand the exact role and relative contribution of hydrophobic interactions and hydrogen bonding. This can be done through an investigation of the thermodynamics and kinetics of the structural evolution. In addition, the rearrangement of hydrogen bond type should be clarified, for example, between peptides or between peptides and water. Future work in this area might explore in more detail the influence of various factors on the Fmoc-FF assembly process, including, solvent type and polarity, the ratio of organic solvent to water, buffer components, solution conditions (ionic

type and valence state, ionic strength, pH) and external conditions (temperature, homogenization method).[9,45]

## 4 | CONCLUSION

By controlling the gelation conditions, Fmoc-FF microspheres were prepared and characterized, potentially allowing new, for example, bioimaging and biosensing applications of these peptide materials, as evidenced through fluorescence imaging and SERS detection of probe molecules in the presence of metal nanoparticles, respectively. The microsphere formation appeared to be governed by changes in the contributions of hydrophobic interactions and hydrogen bonding. Raman and FTIR spectroscopy provided evidence of a modified structure, supported by simulation. Furthermore, the bandgap could be tuned, as evidenced by UV–vis data, a feature that might be exploited to enhance charge transfer in SERS detection. Finally, the increased lifetimes were correlated with reduced bandgap, suggestive of a charge transfer mechanism that might also increase the stability of an excited state of a probe molecule. The observed increase in a lifetime could be due to a semiconductor-induced charge transfer process, allowing extended lifetime for the excited singlet state between Fmoc-FF and TMPyP.

## CONFLICT OF INTEREST STATEMENT

The authors declare no conflict of interest.

## DATA AVAILABILITY STATEMENT

The data that support the findings of this study are available from the corresponding authors upon reasonable request.

## ORCID

*Sawsan Almohammed* https://orcid.org/0000-0002-5990-5088
*Brian J. Rodriguez* https://orcid.org/0000-0001-9419-2717

## REFERENCES

[1] G. Fichman, T. Guterman, J. Damron, L. Adler-Abramovich, J. Schmidt, E. Kesselman, L. J. W. Shimon, A. Ramamoorthy, Y. Talmon, E. Gazit, *Sci. Adv.* **2016**, *2*, e1500827.

[2] V. Basavalingappa, S. Bera, B. Xue, J. O'Donnell, S. Guerin, P. A. Cazade, H. Yuan, E. U. Haq, C. Silien, K. Tao, L. J. W. Shimon, S. A. M. Tofail, D. Thompson, S. Kolusheva, R. Yang, Y. Cao, E. Gazit, *ACS Nano* **2020**, *14*, 7025.

[3] S. Almohammed, M. Alruwaili, E. G. Reynaud, G. Redmond, J. H. Rice, B. J. Rodriguez, *ACS Appl. Nano Mater.* **2019**, *2*, acsanm.9b00940.

[4] C. Diaferia, G. Morelli, A. Accardo, *J. Mater. Chem. B* **2019**, *7*, 5142.

[5] N. A. Dudukovic, C. F. Zukoski, *Soft Matter* **2015**, *11*, 7663.

[6] X. Yan, P. Zhu, J. Li, *Chem. Soc. Rev.* **2010**, *39*, 1877.

[7] C. Diaferia, E. Rosa, G. Morelli, A. Accardo, *Pharmaceuticals* **2022**, *15*, 10.

[8] R. Ischakov, L. Adler-Abramovich, L. Buzhansky, T. Shekhter, E. Gazit, *Bioorg. Med. Chem.* **2013**, *21*, 3517.

[9] K. Tao, A. Levin, L. Adler-Abramovich, E. Gazit, *Chem. Soc. Rev.* **2016**, *45*, 3935.

[10] M. Amit, S. Yuran, E. Gazit, M. Reches, N. Ashkenasy, *Adv. Mater.* **2018**, *30*, 1.

[11] J. H. Kim, D. H. Nam, Y. W. Lee, Y. S. Nam, C. B. Park, *Small* **2014**, *10*, 1272.

[12] D. Mandal, A. Nasrolahi Shirazi, K. Parang, *Org. Biomol. Chem.* **2014**, *12*, 3544.

[13] H. Erdogan, M. Yilmaz, E. Babur, M. Duman, H. M. Aydin, G. Demirel, *Biomacromolecules* **2016**, *17*, 1788.

[14] F. Paladini, S. T. Meikle, I. R. Cooper, J. Lacey, V. Perugini, M. Santin, *J. Mater. Sci. Mater. Med.* **2013**, *24*, 2461.

[15] L. Adler-Abramovich, N. Kol, I. Yanai, D. Barlam, R. Z. Shneck, E. Gazit, I. Rousso, *Angew. Chem.* **2010**, *122*, 10135.

[16] G. Pandit, K. Roy, U. Agarwal, S. Chatterjee, *ACS Omega* **2018**, *3*, 3143.

[17] Z. A. Arnon, D. Pinotsi, M. Schmidt, S. Gilead, T. Guterman, A. Sadhanala, S. Ahmad, A. Levin, P. Walther, C. F. Kaminski, M. Fändrich, G. S. Kaminski Schierle, L. Adler-Abramovich, L. J. W. Shimon, E. Gazit, *ACS Appl. Mater. Interfaces* **2018**, *10*, 20783.

[18] A. K. Gaharwar, N. A. Peppas, A. Khademhosseini, *Biotechnol. Bioeng.* **2014**, *111*, 441.

[19] M. A. Ziganshin, R. A. Larionov, A. V. Gerasimov, S. A. Ziganshina, A. E. Klimovitskii, K. R. Khayarov, T. A. Mukhametzyanov, V. V. Gorbatchuk, *J. Pept. Sci.* **2019**, *25*, 25.

[20] W. Ji, C. Yuan, P. Chakraborty, P. Makam, S. Bera, S. Rencus-Lazar, J. Li, X. Yan, E. Gazit, *ACS Nano* **2020**, *14*, 7181.

[21] C. Yuan, A. Levin, W. Chen, R. Xing, Q. Zou, T. W. Herling, P. K. Challa, T. P. J. Knowles, X. Yan, *Angew. Chemie – Int. Ed.* **2019**, *58*, 18116.

[22] R. M. F. Baptista, P. E. Lopes, A. R. O. Rodrigues, N. Cerca, M. S. Belsley, E. de Matos Gomes, *Mater. Adv.* **2022**, *3*, 2934.

[23] J. Wang, C. Yuan, Y. Han, Y. Wang, X. Liu, S. Zhang, X. Yan, *Small* **2017**, *13*, 1.

[24] R. Contreras-Montoya, A. B. Bonhome-Espinosa, A. Orte, D. Miguel, J. M. Delgado-López, J. D. G. Duran, J. M. Cuerva, M. T. Lopez-Lopez, L. Á. De Cienfuegos, *Mater. Chem. Front.* **2018**, *2*, 686.

[25] C. Yuan, W. Ji, R. Xing, J. Li, E. Gazit, X. Yan, *Nat. Rev. Chem.* **2019**, *3*, 567.

[26] L. Adler-Abramovich, D. Aronov, E. Gazit, G. Rosenman, *J. Nanosci. Nanotechnol.* **2009**, *9*, 1701.

[27] N. A. Dudukovic, C. F. Zukoski, *J. Chem. Phys.* **2014**, *141*, 164905.

[28] A. Heredia, I. Bdikin, S. Kopyl, E. Mishina, S. Semin, A. Sigov, K. German, V. Bystrov, J. Gracio, A. L. Kholkin, *J. Phys. D. Appl. Phys.* **2010**, *43*, 43.

[29] S. Almohammed, A. Fularz, M. B. Kanoun, S. Goumri-Said, A. Aljaafari, B. J. Rodriguez, J. H. Rice, *ACS Appl. Mater. Interfaces* **2022**, *14*, 12504.

[30] S. Smidstrup, T. Markussen, P. Vancraeyveld, J. Wellendorff, J. Schneider, T. Gunst, B. Verstichel, D. Stradi, P. A. Khomyakov, U. G. Vej-Hansen, M. E. Lee, S. T. Chill, F. Rasmussen, G. Penazzi, F. Corsetti, A. Ojanperä, K. Jensen, M. L. N. Palsgaard, U. Martinez, A. Blom, M. Brandbyge, K. Stokbro, *J. Phys. Condens. Matter* **2020**, *32*, 1.

[31] J. P. Perdew, K. Burke, M. Ernzerhof, *Phys. Rev. Lett.* **1997**, *78*, 1396.

[32] M. J. van Setten, M. Giantomassi, E. Bousquet, M. J. Verstraete, D. R. Hamann, X. Gonze, G. M. Rignanese, *Comput. Phys. Commun.* **2018**, *226*, 39.

[33] L. Adler-Abramovich, E. Gazit, *Chem. Soc. Rev.* **2014**, *43*, 6881.

[34] J. T. van Herpt, M. C. A. Stuart, W. R. Browne, B. L. Feringa, *Langmuir* **2013**, *29*, 8763.

[35] J. Raeburn, C. Mendoza-Cuenca, B. N. Cattoz, M. A. Little, A. E. Terry, A. Zamith Cardoso, P. C. Griffiths, D. J. Adams, *Soft Matter* **2015**, *11*, 927.

[36] Y. Gong, X. Chen, Y. Lu, W. Yang, *Biosens. Bioelectron.* **2015**, *66*, 392.

[37] A. Fularz, S. Almohammed, J. H. Rice, *J. Phys. Chem. C* **2020**, *124*, 25351.

[38] S. Almohammed, K. Orhan, S. Daly, D. D. O'Regan, B. J. Rodriguez, E. Casey, J. H. Rice, *JACS Au* **2021**, *1*, 1987.

[39] T. Andrade-Filho, F. F. Ferreira, W. A. Alves, A. R. Rocha, *Phys. Chem. Chem. Phys.* **2013**, *15*, 7555.

[40] T. Li, X.-M. Lu, M.-R. Zhang, K. Hu, Z. Li, *Bioact. Mater.* **2021**, *11*, 268.

[41] Y. Pan, W. Wang, S. Guo, S. Jin, E. Park, Y. Sun, L. Chen, Y. M. Jung, *Chemosensors* **2021**, *9*, 111.

[42] P. Miao, J. Wu, Y. Du, Y. Sun, P. Xu, *J. Mater. Chem. C* **2018**, *6*, 10855.

[43] S. Takagi, M. Eguchi, D. A. Tryk, H. Inoue, *J. Photochem. Photobiol. C Photochem. Rev.* **2006**, *7*, 104.

[44] M. Reches, E. Gazit, *Nat. Nanotechnol.* **2006**, *1*, 195.

[45] V. Basavalingappa, T. Guterman, Y. Tang, S. Nir, J. Lei, P. Chakraborty, L. Schnaider, M. Reches, G. Wei, E. Gazit, *Adv. Sci.* **2019**, *6*, 1900218.

## SUPPORTING INFORMATION

Additional supporting information can be found online in the Supporting Information section at the end of this article.